Supplementary information for:

Constraining African Wildfire Carbon Emissions Using Satellite XCO_2 Retrievals

Guoyuan Lv[1], Fei Jiang[1,2,6*], Shuzhuang Feng[1], Yongguang Zhang[1], Guanyu Dong[1], Jun Wang[1], Mousong Wu[1], Yusheng Shi[3], Hengmao Wang[1], Mengwei Jia[1], Lingyu Zhang[1], Yu Mao[1], Weimin Ju[1,6], Jing M. Chen[4,5]

[1] Jiangsu Provincial Key Laboratory of Geographic Information Science and Technology, International Institute for Earth System Science, Nanjing University, Nanjing, 210023, China.

[2] Frontiers Science Center for Critical Earth Material Cycling, Nanjing University, Nanjing, 210023, China.

[3] Aerospace Information Research Institute, Chinese Academy of Sciences, Beijing, 100094, China.

[4] Department of Geography and Planning, University of Toronto, Toronto, Ontario M5S3G3, Canada.

[5] School of Geographical Sciences, Fujian Normal University, Fuzhou, 350007, China.

[6] Jiangsu Center for Collaborative Innovation in Geographical Information Resource Development and Application, Nanjing, 210023, China.

Corresponding author: Fei Jiang (jiangf@nju.edu.cn)

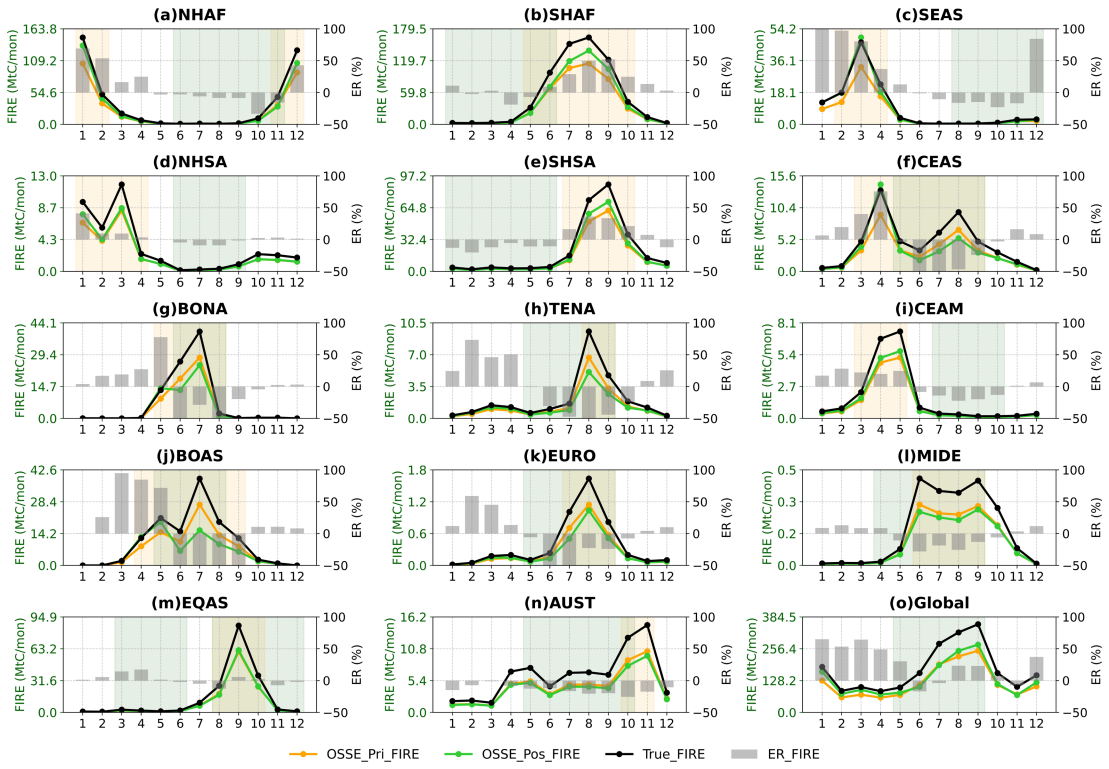

Supplementary Fig. 1: Monthly wildfire carbon (FIRE) emissions and error reduction (ER) across 14 global regions in the OSSE experiment. Regional classifications follow the GFED4s framework: BONA (Boreal North America), TENA (Temperate North America), CEAM (Central America), NHSA (Northern Hemisphere South America), SHSA (Southern Hemisphere South America), EURO (Europe), MIDE (Middle East), NHAF (Northern Hemisphere Africa), SHAF (Southern Hemisphere Africa), BOAS (Boreal Asia), CEAS (Central Asia), SEAS (Southeast Asia), EQAS (Equatorial Asia), and AUST (Australia). Orange shading highlights wildfire seasons, while green shading represents the vegetation growing season.

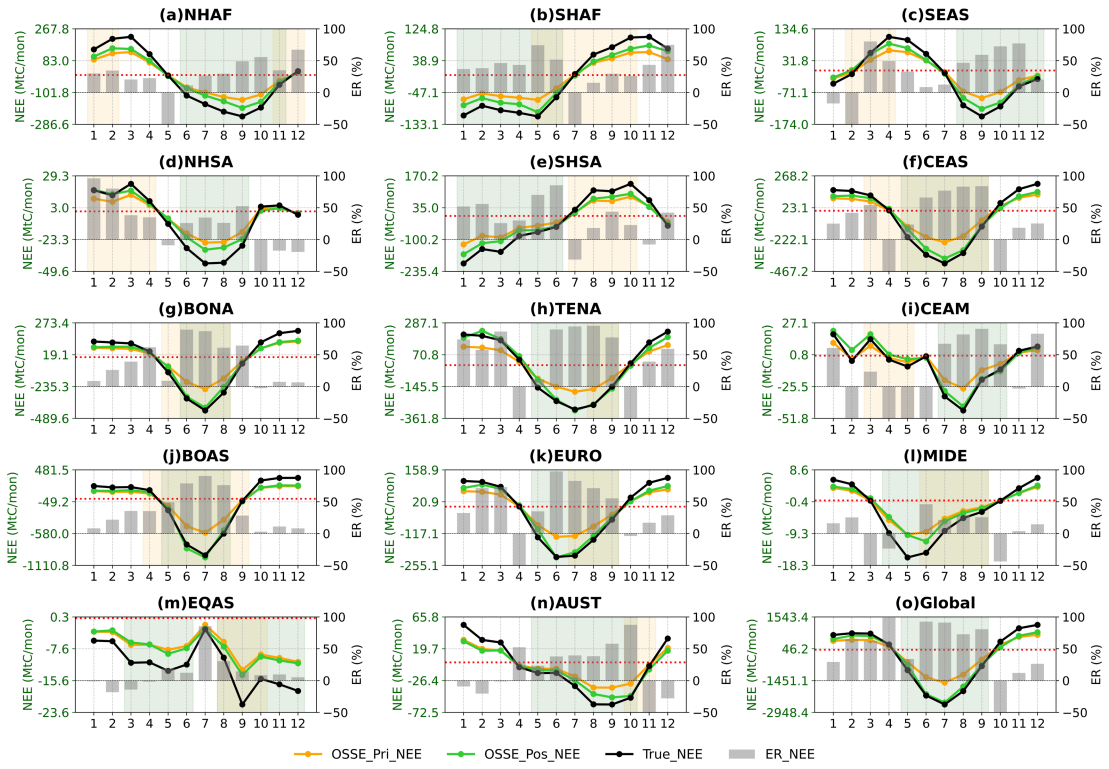

Supplementary Fig. 2: Monthly net ecosystem exchange (NEE) and corresponding error reduction (ER) across 14 global regions in 2015 and 2016 from the OSSE experiment. Regional classifications follow the GFED4s framework, consistent with Fig.1. Orange shading highlights wildfire seasons, while green shading represents the vegetation growing season.

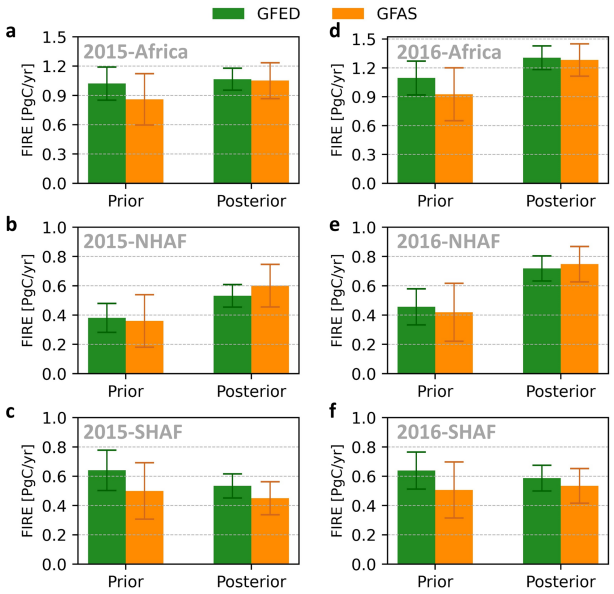

Supplementary Fig. 3: Comparison of prior and posterior wildfire carbon emissions for 2015 and 2016 in the inversion experiments. Panels (a) and (d) represent total emissions across sub-Saharan Africa, (b) and (e) correspond to NHAF region, and (c) and (f) correspond to SHAF.

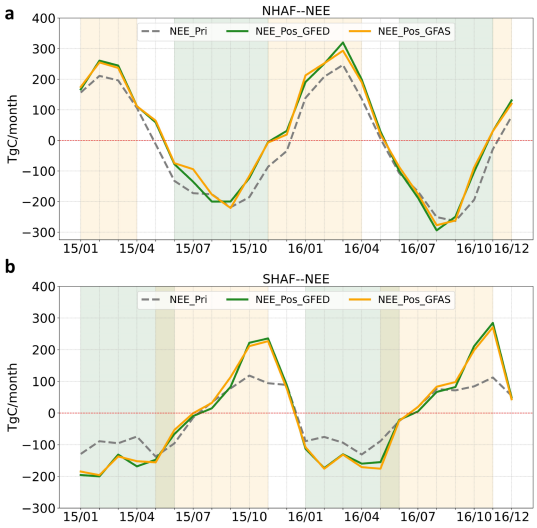

Supplementary Fig. 4: Prior and posterior monthly NEE fluxes in NHAF and SHAF for 2015 and 2016, respectively. Orange-shaded marks wildfire seasons, while green-shaded indicates strong vegetation carbon uptake periods.

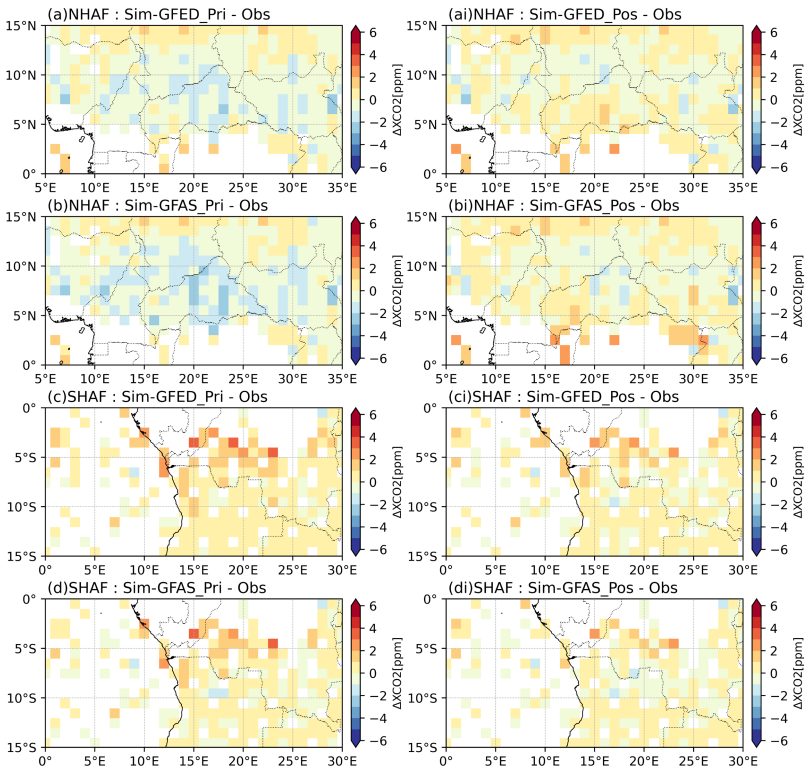

Supplementary Fig. 5: Comparison of OCO-2 XCO_2 observations and simulations for NHAF (January and December 2015–2016) and SHAF (July and August 2015, June and July 2016) during months of greatest FIRE variability. The first row corresponds to NHAF, and the second row represents SHAF.

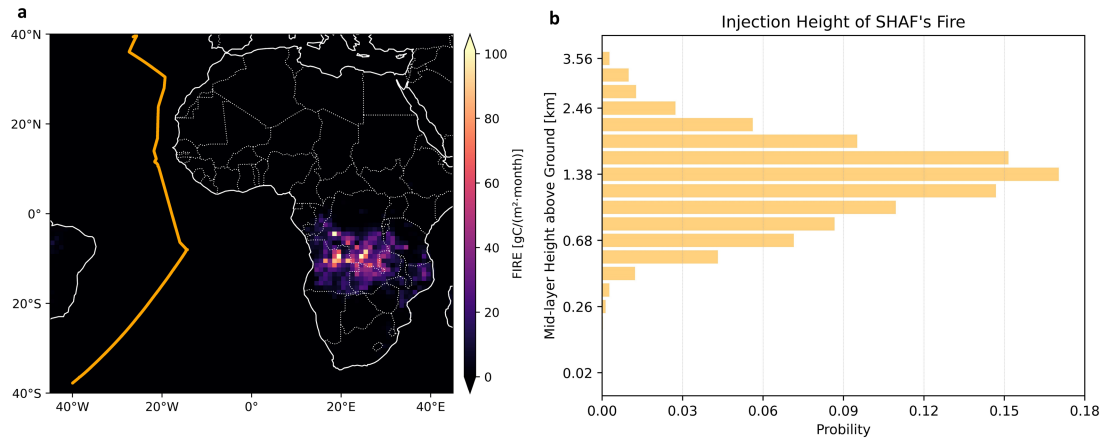

Supplementary Fig. 6: The setup of CMAQ model. (a) CMAQ simulation domain and the GFED4s wildfire carbon emissions for sub-Saharan Africa in 2016 August, with ATom-1 aircraft routes shown in orange. (b) Wildfire plume injection heights over SHAF from CAMS-GFAS.

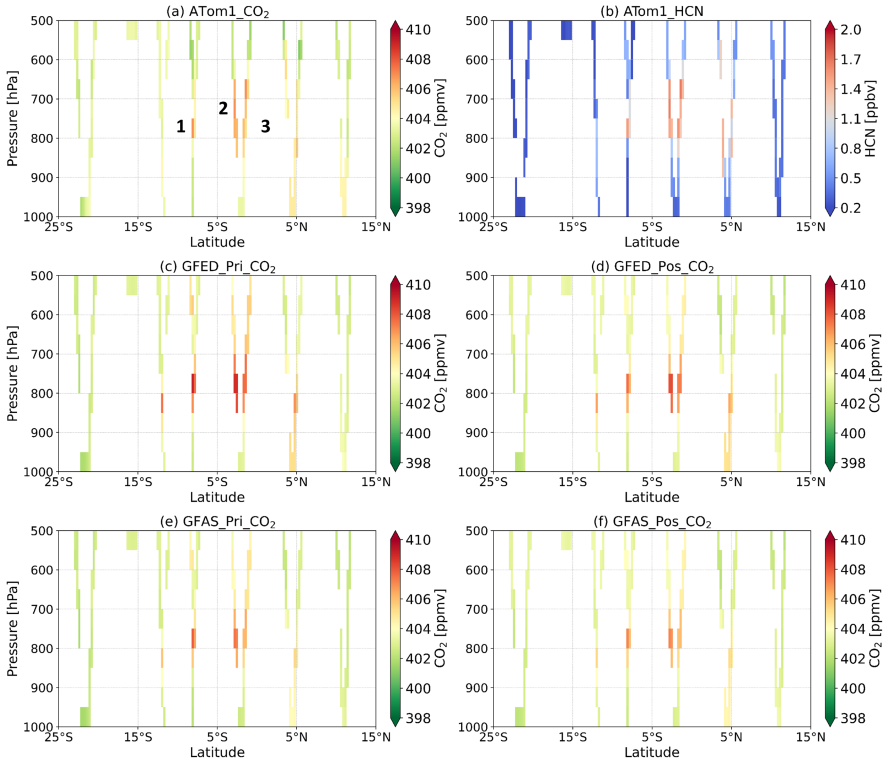

Supplementary Fig. 7: Evaluation of simulated CO_2 mixing ratios against the Atom-1 Airborne observations. (a) ATom-1 CO_2 mixing ratio observations; (b) ATom-1 HCN mixing ratio observations; (c, d) simulated CO_2 mixing ratios in experiment TIN1 before and after optimization; (e, f) simulated CO_2 mixing ratios in experiment TIN2 before and after optimization. All data are sampled at a horizontal resolution of 27 km resolution and vertically binned into 50 hPa pressure intervals.

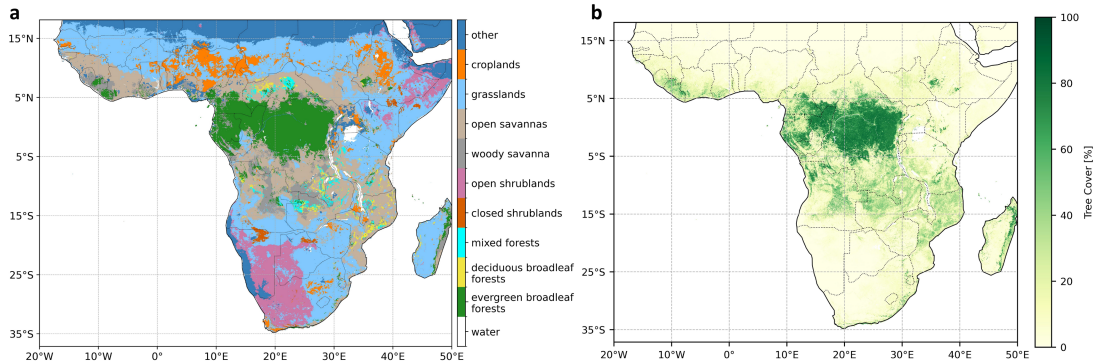

Supplementary Fig. 8: Landscape characteristic of Africa. (a) Land cover classification from MODIS MCD12Q1 (IGBP scheme) and (b) tree cover fraction derived from MOD44B. Both maps are presented at 0.05° spatial resolution.

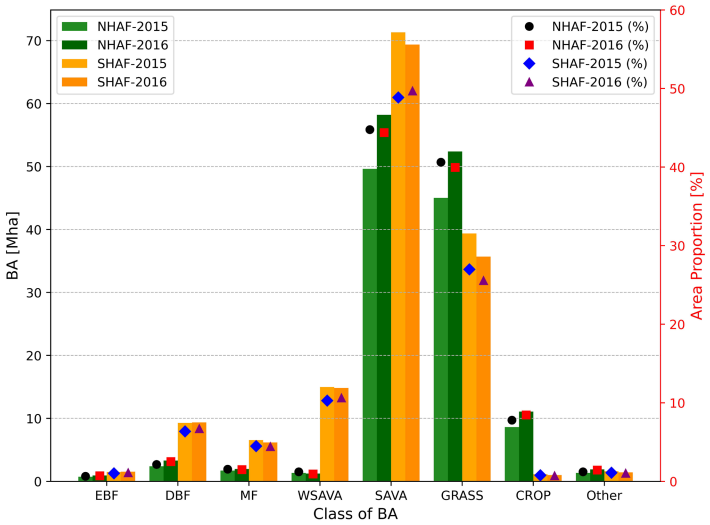

Supplementary Fig. 9: Burned area (BA) across different land cover classes in the NHAF and SHAF regions for 2015 and 2016. The data derived from MODIS MCD64A1 collection 6 products. Land cover classes include evergreen broadleaf forests (EBF), deciduous broadleaf forests (DBF), mixed forests (MF), woody savannas (WSAVA), savannas (SAVA), grasslands (GRASS), croplands (CROP), and other types (other).

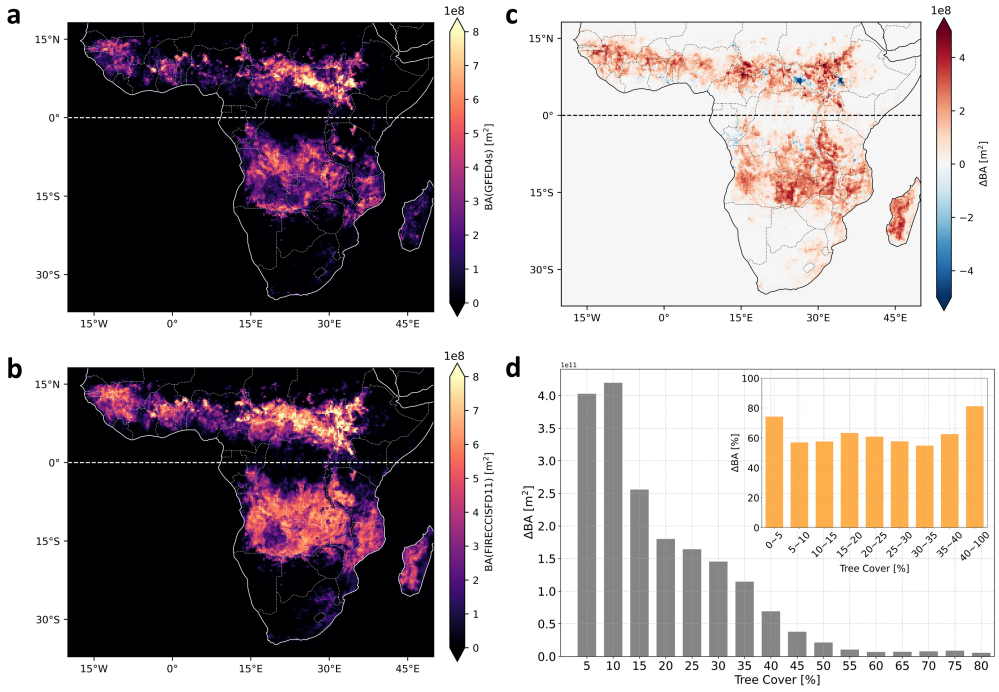

Supplementary Fig. 10: Spatial distributions and comparative analysis of burned area (BA) estimates across Africa at 0.25° in 2016. (a) GFED4s-derived BA. (b) FireCCISFD11-derived BA. (c) Difference between FireCCISFD11 and GFED4s BA estimates (FireCCIS51 minus GFED4s). (d) Relationship between tree cover (%) and difference in BA estimates (ΔBA) between FireCCISFD11 and GFED4s.

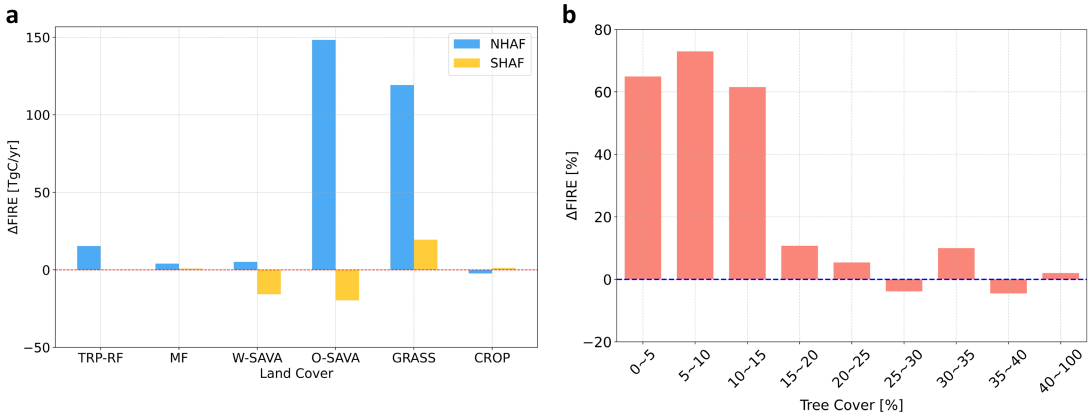

Supplementary Fig. 11: Comparison of posterior and prior wildfire carbon (FIRE) emissions from GFAS across different landscapes in NHAF and SHAF. (a) Total adjustments in FIRE emissions (ΔFIRE [TgC/yr]) between posterior and prior estimates from GFED4s, aggregated by major land cover types in NHAF and SHAF: tropical rainforest (Trp-RF), woody savannas (W-SAVA), open savannas (O-SAVA), grasslands (GRASS) and cropland (CROP). The Trp-RF category includes evergreen broadleaf forest and deciduous broadleaf forest. (b) Relationship between relative FIRE emission adjustment (ΔFIRE [%]) and tree cover, categorized into 5% intervals up to 40%.

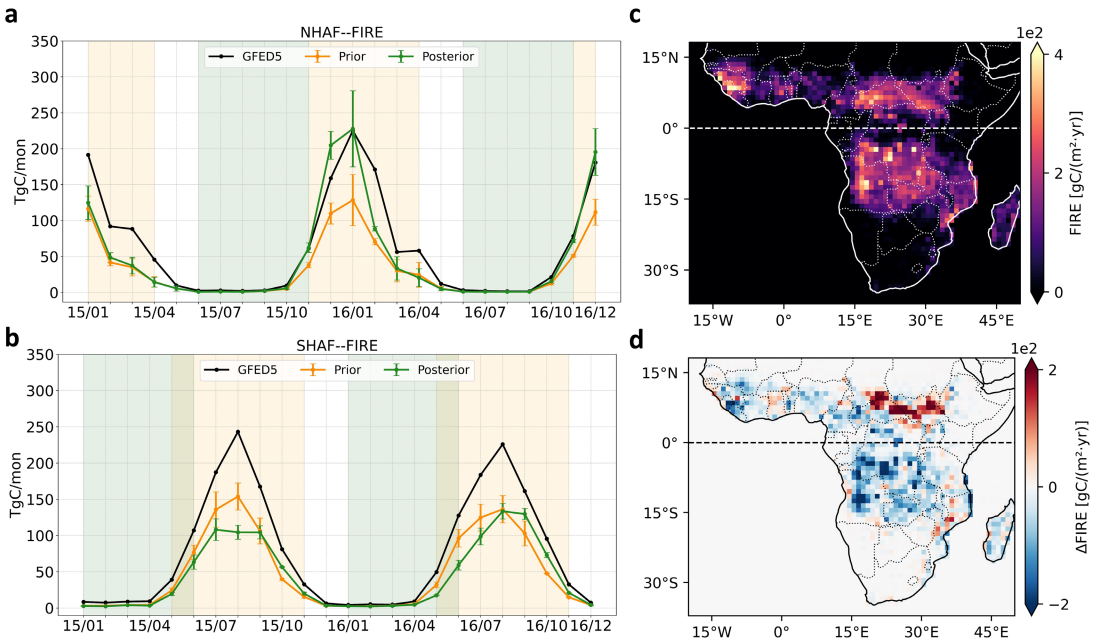

Supplementary Fig. 12: Comparison of wildfire carbon (FIRE) emissions between our inversion results and GFED5. Panels (a, b) illustrate the monthly evolution of prior and posterior FIRE emissions from our inversion alongside GFED5 wildfire Carbon emissions in NHAF and SHAF, respectively. Panels (c, d) presents the annual GFED5 FIRE emissions and the corresponding differences between our inversion estimates and GFED5, respectively.